Available online at www.sciencedirect.com
SCIENCE DIRECT®
PERGAMON
International Journal of Heat and Mass Transfer 46 (2003) 1811–1825
International Journal of HEAT and MASS TRANSFER
www.elsevier.com/locate/ijhmt

Large eddy simulation of heat and mass transport in turbulent flows. Part 1: Velocity field

Farhad A. Jaberi [a,*], Paul J. Colucci [b]

[a] Department of Mechanical Engineering, Michigan State University, East Lansing, MI 48824-1226, USA
[b] Fluent Inc., Ann Arbor, MI 48104, USA

Received 29 January 2002; received in revised form 7 November 2002

Abstract

Localized residual or subgrid-scale (SGS) models are presented for use in large eddy simulation of heat and mass transport in turbulent flows. In part (1) (this paper), we discuss the SGS stress models for the velocity field. The models for the scalar field are presented in part (2). The new SGS stress closures are compared with the dynamic-Smagorinsky model (DSM) and the dynamic two-parameter mixed model (DTMM). All models are applied "locally" and their performances are assessed via both a priori and a posteriori analyses with detailed comparisons against data obtained from direct numerical simulation of homogeneous isotropic, homogeneous shear and temporal mixing layer flows. The results of a priori assessments indicate that the new closures predict the SGS stresses better than both DSM and DTMM in all simulated flows. The results of a posteriori assessments also show that the SGS stresses and the statistics of the filtered velocity are more accurately predicted with the new models.

1. Introduction

Among various numerical methodologies available for prediction of heat and mass transport in turbulent flows, large eddy simulation (LES) appears to be very promising [1,2]. LES can generate a time- and space-accurate "realistic" solution provided that the unclosed subgrid-scale (SGS) closures are accurately modeled. These closures represent: (1) the SGS velocity–velocity correlations (stresses), (2) the SGS velocity–scalar correlations (scalar fluxes), and (3) the SGS scalar–scalar correlations (unmixedness). The physical behavior and modeling of the SGS stresses are discussed here. The SGS scalar flux and unmixedness are considered in Ref. [3].

One of the most established models in LES is the eddy-viscosity-based closure of Smagorinsky [4]. In this closure, the SGS Reynolds stresses are related to the large scale strain rate, and the eddy viscosity is evaluated based on the assumption that the SGS energy production and dissipation are in equilibrium. This model and its variants have been widely used in LES [5,6] and its fair success is attributed to its ability to predict the global SGS dissipation correctly [7]. Despite its popularity, the model has some drawbacks [7–9]. To overcome some of these drawbacks Bardina et al. [7] proposed a "scale-similarity" model in which double filtering is utilized to evaluate the SGS stresses from the dynamics of the resolved field. Comparison with direct numerical simulation (DNS) and experimental data indicates that the scale-similarity model is more accurate than the Smagorinsky closure [7,9].

The concept of double filtering is further extended in the "dynamic-Smagorinsky" model (DSM), [10,11], in which a dynamic procedure is used to evaluate the Smagorinsky "constant". Associated with DSM are possible numerical instabilities that may occur when the local formulation of the model is implemented. Also, the SGS stresses predicted by this model correlate poorly with the SGS stresses obtained from DNS data [12,13]. In practice, DSM is almost always dissipative, both in a

* Corresponding author. Tel.: +1-517-432-4678; fax: +1-517-353-1750.
E-mail address: jaberi@egr.msu.edu (F.A. Jaberi).

0017-9310/03/$ - see front matter
doi:10.1016/S0017-9310(02)00484-2

Nomenclature

C_{ij}	cross part of subgrid-scale stress tensor
k	magnitude of the Fourier wavenumber
$k_{\max}$	maximum Fourier wavenumber
L_{ij}	Leonard part of subgrid-scale stress tensor
p	pressure
R_{ij}	Reynolds part of subgrid-scale stress tensor
Re_0	reference Reynolds number
Re_λ	Taylor micro-scale Reynolds number
S	magnitude of rate of strain tensor
$\overline{S}_{ij}$	mean rate of strain tensor
t	time
T_{ij}	residual stress tensor at test-level
u_i	ith component of the fluid velocity vector
$u_{\rm rms}$	rms of turbulent velocity
x_i	Cartesian coordinates ($x_1 = x$, $x_2 = y$, $x_3 = z$).

Greek symbols

α	ratio of grid-level to test-level filter sizes
δx	grid spacing
$\overline{\Delta}$	characteristic size of the grid-level filter
$\widehat{\Delta}$	characteristic size of the test-level filter
ϵ	dissipation rate of turbulent kinetic energy
η	Kolmogorov length scale
ν_t	subgrid-scale viscosity
ρ	correlation coefficient
τ_{ij}	subgrid-scale stress tensor

Superscripts

$\overline{\ }$	grid-level filtering operator
$\widehat{\ }$	test-level filtering operator
$'$	subgrid-scale fluctuations

volume (or plane) averaged formulation in which a net positive Smagorinsky coefficient is obtained [10], and in a localized formulation in which the model coefficient is constrained to positive values [14]. Some improvement of DSM is suggested by Salvetti and Banerjee [12] who propose a dynamic two-parameter mixed model (DTMM), in which the "generalized cross" term is assumed to be proportional to the "generalized Leonard" term, and the "generalized Reynolds" term is represented by the Smagorinsky closure. The generalized terms are subparts of the SGS stress tensor according to the Germano's decomposition [11]. Improved versions of DSM are also proposed by Germano [15] and others.

In this work, we propose two new SGS closure strategies for LES. The first, termed the sequential or serial decomposition (SDC) model is based on decomposition of the generalized Leonard (**L**), cross (**C**) and Reynolds (**R**) components of the SGS stresses into sequential "Leonard", "cross" and "Reynolds" terms of their own. The unclosed components of those sequential terms are modeled. The second, referred to as the direct correlation (DC) closure is based on the assumptions that the local values of **C** and **R** are highly correlated with the "Leonard" part of **R**. Both closures are applied "locally" and the predicted LES results are compared with those via other models. The performance of the new closures is also determined by detailed comparisons with DNS data by means of both a priori and a posteriori analyses. This is done by considering several turbulent flow configurations with a variety of different conditions and operational parameters. Each of these two closures can be enacted in several different ways. Two ways of implementing the SDC and one way of using DC are demonstrated in this paper.

2. Mathematical considerations and modeling

For LES of a constant (unit) density, Newtonian fluid, the starting point is the normalized filtered Navier–Stokes equations (repeated index imply summation),

$$\frac{\partial(\overline{u}_j)}{\partial x_j} = 0, \tag{1}$$

$$\frac{\partial \overline{u}_i}{\partial t} + \frac{\partial(\overline{u}_i\overline{u}_j)}{\partial x_j} = -\frac{\partial \overline{p}}{\partial x_i} - \frac{\partial \tau_{ij}}{\partial x_j} + \frac{1}{Re_0}\frac{\partial^2 \overline{u}_i}{\partial x_j \partial x_j}, \tag{2}$$

where u_i is the fluid velocity in x_i direction, p is the fluid pressure, t represents time, and the overbar denotes the grid-level convolution filtered value [16,14]. The variables are normalized using the reference length (L_0), velocity (U_0), and density (ρ_0) scales. Consequently, the important non-dimensional parameter is the Reynolds number ($Re_0 = \rho_0 U_0 L_0/\mu$, where μ is the fluid viscosity). The closure problem in Eq. (2) is associated with the SGS stress tensor, $\tau_{ij} = \overline{u_i u_j} - \overline{u}_i\overline{u}_j$.

As suggested by Kerr et al. [17], models which make use of the dynamics of the resolved field are potentially more successful than those based on the derivative of the resolved velocity scales. Germano et al. [10] effectively make use of the resolved field by defining a test-scale filter operator (denoted by a "hat"). The application of this filter to Eqs. (1) and (2), yields another unclosed term, $T_{ij} = \widehat{\overline{u_i u_j}} - \widehat{\overline{u}}_i\widehat{\overline{u}}_j$, termed the "subtest-scale" stress tensor. The stresses at the grid- (τ_{ij}) and the test-levels (T_{ij}) are related by,

$$G_{ij} = T_{ij} - \widehat{\tau_{ij}} = \widehat{\overline{u_i u_j}} - \widehat{\overline{u}}_i\widehat{\overline{u}}_j. \tag{3}$$

Eq. (3) known as the Germano's identity, holds for any approximation of $\overline{u_i u_j}$.

In the Smagorinsky closure the anisotropic part of τ_{ij} is assumed to be proportional to resolved rate of strain tensor, $\overline{S}_{ij}$ through the turbulent diffusivity coefficient (ν_t):

$$\tau_{ij} - \frac{\delta_{ij}}{3}\tau_{kk} \approx -2\nu_t \overline{S}_{ij}, \tag{4}$$

$$\nu_t = c_s \overline{\Delta}^2 |\overline{S}|, \quad |\overline{S}| = (2\overline{S}_{ij}\overline{S}_{ij})^{1/2}, \quad \overline{S}_{ij} = \frac{1}{2}\left(\frac{\partial \overline{u}_i}{\partial x_j} + \frac{\partial \overline{u}_j}{\partial x_i}\right),$$

where c_s is the Smagorinsky constant and $\overline{\Delta}$ is the characteristic length scale of the filter at the grid-level. A positive value of c_s insures a positive value for SGS dissipation ($\epsilon = -\tau_{ij}\overline{S}_{ij}$). In DSM, the anisotropic part of T_{ij} is similarly approximated by the Smagorinsky closure. Substitution of the models for τ_{ij} and T_{ij} into the Germano identity (Eq. (3)) and utilization of a least square error minimization technique results in an expression for c_s [18].

Following Germano [11], τ_{ij} is decomposed into

$$\tau_{ij} = L_{ij} + C_{ij} + R_{ij} \tag{5}$$

$$L_{ij} = \overline{\overline{u}_i \overline{u}_j} - \overline{\overline{u}}_i \overline{\overline{u}}_j,$$
$$C_{ij} = (\overline{\overline{u}_i u'_j} - \overline{\overline{u}}_i \overline{u'}_j) + (\overline{u'_i \overline{u}_j} - \overline{u'}_i \overline{\overline{u}}_j),$$
$$R_{ij} = \overline{u'_i u'_j} - \overline{u'}_i \overline{u'}_j,$$

where $u'_i = u_i - \overline{u}_i$ and L_{ij}, C_{ij} and R_{ij} are referred to "generalized Leonard term", "generalized cross term" and "generalized Reynolds term", respectively (for brevity the word generalized is dropped hereinafter). As explained by Germano [11], with the application of a linear filter which commutes with time and space, the filtered Navier–Stokes equations must remain invariant in terms of the generalized central moments. Thus, the Leonard, cross, and Reynolds substresses must retain the properties of the original stress and in particular they must be Galilean invariant. These new stresses are expected to constitute a significant part of the SGS stress tensor when a filter allowing an overlap between the resolved and unresolved scales is used. A similar decomposition can be made at the test-level for T_{ij}.

2.1. The serial decomposition closure

With the decomposition in Eq. (5), L_{ij} can be evaluated explicitly, while C_{ij} and R_{ij} need to be modeled. In the dynamic mixed model of Zang et al. [19], the Smagorinsky closure is employed for $C_{ij} + R_{ij}$. In DTMM of Salvetti and Banerjee [12], C_{ij} is assumed to be proportional to L_{ij} and the Smagorinsky closure is employed for R_{ij}.

The model proposed here is based on the fact that C_{ij} and R_{ij} contain some information about the resolved field which do not require modeling. Therefore, with the "SDC" of these stresses, only the terms pertaining to the unresolved field are modeled. The decomposition involves the use of $u_i = \overline{u}_i + u'$ in the Eq. (5);

$$\begin{aligned} C_{ij} = {} & \underbrace{(\overline{\overline{u}_i \overline{u}'_j} - \overline{\overline{u}}_i \overline{\overline{u}}_j) + (\overline{\overline{u}'_i \overline{u}_j} - \overline{\overline{u}'}_i \overline{\overline{u}}_j)}_{\text{(I)}} \\ & + \underbrace{(\overline{\overline{u}_i (u'_j)'} - \overline{\overline{u}}_i \overline{(u'_j)'}) + (\overline{(u'_i)' \overline{u}_j} - \overline{(u'_i)'} \overline{\overline{u}}_j)}_{\text{(II)}} \\ & + \underbrace{2(\overline{\overline{u}'_i \overline{u}'_j} - \overline{\overline{u}'}_i \overline{\overline{u}'}_j)}_{\text{(III)}} \\ & + \underbrace{(\overline{\overline{u}'_i (u'_j)'} - \overline{\overline{u}'}_i \overline{(u'_j)'}) + (\overline{(u'_i)' \overline{u}'_j} - \overline{(u'_i)'} \overline{\overline{u}'}_j)}_{\text{(IV)}} \end{aligned} \tag{6}$$

$$\begin{aligned} R_{ij} = {} & \underbrace{(\overline{\overline{u}'_i \overline{u}'_j} - \overline{\overline{u}'}_i \overline{\overline{u}'}_j)}_{\text{(V)}} \\ & + \underbrace{(\overline{\overline{u}'_i (u'_j)'} - \overline{\overline{u}'}_i \overline{(u'_j)'}) + (\overline{(u'_i)' \overline{u}'_j} - \overline{(u'_i)'} \overline{\overline{u}'}_j)}_{\text{(VI)}} \\ & + \underbrace{(\overline{(u'_i)' (u'_j)'} - \overline{(u'_i)'} \overline{(u'_j)'})}_{\text{(VII)}}, \end{aligned} \tag{7}$$

where $(u'_i)' \equiv u'_i - \overline{u'_i} = u_i - 2\overline{u_i} + \overline{\overline{u_i}}$. Terms (I), (III) in Eq. (6) and the term (V) in Eq. (7) can be evaluated explicitly. The Leonard and the cross parts of R_{ij} in Eq. (7) (terms (V) and (VI)) are the same as terms (III) and (IV) in Eq. (6). This suggests that there should be a reasonable correlation between C_{ij} and R_{ij} (as indeed confirmed by a priori analysis discussed below).

Substituting Eqs. (6) and (7) into Eq. (5) yields

$$\tau_{ij} = \phi_{ij} + \psi_{ij}, \tag{8}$$

where ϕ_{ij} and ψ_{ij}, the "known" and "unknown" parts of SGS stresses, are defined as

$$\begin{aligned} \phi_{ij} = {} & (\overline{\overline{u}_i \overline{u}_j} - \overline{\overline{u}}_i \overline{\overline{u}}_j) + (\overline{\overline{u}_i \overline{u}'_j} - \overline{\overline{u}}_i \overline{u}'_j + \overline{u'_i \overline{u}_j} - \overline{u'}_i \overline{\overline{u}}_j) \\ & + 3(\overline{\overline{u}'_i \overline{u}'_j} - \overline{\overline{u}'}_i \overline{\overline{u}'}_j) \\ = {} & (\overline{\overline{u}_i \overline{u}_j} - \overline{\overline{u}}_i \overline{\overline{u}}_j) + (\overline{\overline{u}_i \overline{u}'_j} - \overline{\overline{u}}_i \overline{\overline{u}'}_j) + (\overline{\overline{u}'_i \overline{u}_j} - \overline{\overline{u}'}_i \overline{\overline{u}}_j) \\ & + (\overline{\overline{u}'_i \overline{u}'_j} - \overline{\overline{u}'}_i \overline{\overline{u}'}_j) \end{aligned}$$

$$\psi_{ij} = (\overline{w_i v_j} - \overline{w}_i \overline{v}_j) + (\overline{v}_i w_j - \overline{v}_i \overline{w}_j),$$

$$w_i = \tfrac{1}{2}(u_i + 2\overline{u}_i - \overline{\overline{u}}_i), \quad v_i = (u'_i)' = u_i - 2\overline{u}_i + \overline{\overline{u}}_i.$$

Similarly, the SGS stress at test-level is decomposed as

$$T_{ij} = \Phi_{ij} + \Psi_{ij} \tag{9}$$

$$\begin{aligned} \Phi_{ij} = {} & (\widehat{\overline{\overline{u}_i \overline{u}_j}} - \widehat{\overline{\overline{u}}}_i \widehat{\overline{\overline{u}}}_j) + (\widehat{\overline{\overline{u}_i \overline{u}'_j}} - \widehat{\overline{\overline{u}}}_i \widehat{\overline{\overline{u}'}}_j) + (\widehat{\overline{\overline{u}'_i \overline{u}_j}} - \widehat{\overline{\overline{u}'}}_i \widehat{\overline{\overline{u}}}_j) \\ & + (\widehat{\overline{\overline{u}'_i \overline{u}'_j}} - \widehat{\overline{\overline{u}'}}_i \widehat{\overline{\overline{u}'}}_j) \end{aligned}$$

$$\Psi_{ij} = (\widehat{\overline{w_i v_j}} - \widehat{\overline{w}}_i \widehat{\overline{v}}_j) + (\widehat{\overline{v}_i w_j} - \widehat{\overline{v}}_i \widehat{\overline{w}}_j).$$

In previous models ϕ_{ij} is either effectively ignored [20] or only partially considered [19]. Here, this term is fully included and ψ_{ij} is modeled. Two models are proposed for this purpose. In the first, the cross and the Reynolds parts of ψ_{ij} are simply neglected:

$$\psi_{ij} \approx \overline{\overline{w}_i\overline{v}_j} - \overline{\overline{w}}_i\overline{\overline{v}}_j + \overline{\overline{v}_i\overline{w}_j} - \overline{\overline{v}}_i\overline{\overline{w}}_j. \tag{10}$$

This model, termed SDC1, is solely based on the convolution property of filters and does not require an input parameter or an adjustable coefficient.

The second model (termed SDC2) is based on the assumption that the cross and the Reynolds parts of ψ_{ij} are proportional to the Leonard part;

$$\psi_{ij} \approx c_1(\overline{\overline{w}_i\overline{v}_j} - \overline{\overline{w}}_i\overline{\overline{v}}_j + \overline{\overline{v}_i\overline{w}_j} - \overline{\overline{v}}_i\overline{\overline{w}}_j), \tag{11}$$

where the model coefficient c_1 is evaluated locally by a dynamic procedure

$$c_1 = \frac{\left(Q_{ij} - \frac{\delta_{ij}}{3}Q_{kk}\right)\left(A_{ij} - \frac{\delta_{ij}}{3}A_{kk}\right)}{\left(A_{ij} - \frac{\delta_{ij}}{3}A_{kk}\right)\left(A_{ij} - \frac{\delta_{ij}}{3}A_{kk}\right)} \tag{12}$$

$$Q_{ij} = \Psi_{ij} - \widehat{\psi_{ij}} = \widehat{\overline{w}_i\overline{v}_j} - \widehat{\overline{w}}_i\widehat{\overline{v}}_j + \widehat{\overline{v}_i\overline{w}_j} - \widehat{\overline{v}}_i\widehat{\overline{w}}_j,$$
$$A_{ij} = \widehat{\overline{\overline{w}}_i\overline{\overline{v}}_j} - \widehat{\overline{\overline{w}}}_i\widehat{\overline{\overline{v}}}_j + \widehat{\overline{\overline{v}}_i\overline{\overline{w}}_j} - \widehat{\overline{\overline{v}}}_i\widehat{\overline{\overline{w}}}_j.$$

In the decomposition of T_{ij}, alternatively it is possible to use $u_i = \widehat{\overline{u}}_i + u_i''$, where u_i'' denotes the test-level velocity fluctuation. This new decomposition is more attractive as it employs the information at test-level to calculate the subtest-scale stresses. With this new decomposition, the expressions for the Leonard, the cross and the Reynolds terms are modified,

$$T_{ij} = \Phi_{ij}^* + \Psi_{ij}^* \tag{13}$$

$$\Phi_{ij}^* = (\widehat{\overline{u}_i\overline{u}_j} - \widehat{\overline{u}}_i\widehat{\overline{u}}_j) + (\widehat{\overline{u}_i\overline{u''}_j} - \widehat{\overline{u}}_i\widehat{\overline{u''}}_j) + (\widehat{\overline{u''}_i\overline{u}_j} - \widehat{\overline{u''}}_i\widehat{\overline{u}}_j) + (\widehat{\overline{u''}_i\overline{u''}_j} - \widehat{\overline{u''}}_i\widehat{\overline{u''}}_j),$$
$$\Psi_{ij}^* = (\widehat{\overline{w_i^*}\overline{v_j^*}} - \widehat{\overline{w^*}}_i\widehat{\overline{v^*}}_j) + (\widehat{\overline{v_i^*}\overline{w_j^*}} - \widehat{\overline{v^*}}_i\widehat{\overline{w^*}}_j).$$
$$w_i^* = \tfrac{1}{2}(u_i + 2\widehat{\overline{u}}_i - \widehat{\overline{u}}_i), \quad v_i^* = u_i - 2\widehat{\overline{u}}_i + \widehat{\overline{u}}_i. \tag{14}$$

By assuming that the cross and the Reynolds part of Ψ_{ij}^* are proportional to its Leonard part,

$$\Psi_{ij}^* \approx c_1^*\left[(\widehat{\overline{w^*}_i\overline{v^*}_j} - \widehat{\overline{w^*}}_i\widehat{\overline{v^*}}_j) + (\widehat{\overline{v^*}_i\overline{w^*}_j} - \widehat{\overline{v^*}}_i\widehat{\overline{w^*}}_j)\right]. \tag{15}$$

This yields a model slightly different than SDC2, labeled SDC2* here.

The unclosed terms in Eq. (8) could be decomposed further. However, the extent of consequent SDCs is limited in practice mainly because the rate of convergence decreases as more stresses are explicitly calculated and/or the overlap between the resolved and the SGSs decreases. Additionally, the cost of added filtering operations could become prohibitive. This issue is discussed further below with some numerical examples.

2.2. The direct correlation closure

The proportionality of C_{ij} to L_{ij} as assumed in DTMM is based on the argument that C_{ij} represents a stress which involves the resolved and unresolved fields and is expected to be dominated by the interactions among the smallest resolved scales and the largest unresolved scales. From the energy cascade theory, a similarity between the flow field in consecutive scales exists and therefore a proportionality between L_{ij} and C_{ij} can be assumed [7,9]. A similar or even an improved correlation between C_{ij} and the Leonard part of R_{ij} ($\mathfrak{R}_{ij}$) in Eq. (7) is expected (see Eqs. (6) and (7)). Therefore, we propose the following dynamic model

$$\tau_{ij} - \frac{\delta_{ij}}{3}\tau_{kk} \approx \left(L_{ij} - \frac{\delta_{ij}}{3}L_{kk}\right) + c_2\left(\mathfrak{R}_{ij} - \frac{\delta_{ij}}{3}\mathfrak{R}_{kk}\right),$$
$$\mathfrak{R}_{ij} = \overline{\overline{u'}_i\overline{u'}_j} - \overline{\overline{u'}}_i\overline{\overline{u'}}_j, \tag{16}$$

where

$$c_2 = \frac{\left(B_{ij} - \frac{\delta_{ij}}{3}B_{kk}\right)\left(D_{ij} - \frac{\delta_{ij}}{3}D_{kk}\right)}{\left(D_{ij} - \frac{\delta_{ij}}{3}D_{kk}\right)\left(D_{ij} - \frac{\delta_{ij}}{3}D_{kk}\right)},$$
$$B_{ij} = (\widehat{\overline{u}_i\overline{u}_j} - \widehat{\overline{u}}_i\widehat{\overline{u}}_j) - (\widehat{\overline{\overline{u}}_i\overline{\overline{u}}_j} - \widehat{\overline{\overline{u}}}_i\widehat{\overline{\overline{u}}}_j),$$
$$D_{ij} = (\widehat{\overline{\overline{u'}}_i\overline{\overline{u'}}_j} - \widehat{\overline{\overline{u'}}}_i\widehat{\overline{\overline{u'}}}_j).$$

This model is labeled DC and is somewhat similar to the one recently proposed by Horiuti [21]. The three models described (SD1, SD2, and DC) are the primary constituents of the proposed SGS closures and are studied in detail. The attributes of these models and those of DSM and DTMM are summarized in Table 1.

Table 1
Summary of the tested SGS stress models

Model	Mathematical description[a] of the model
DSM	$-2c_s\overline{\Delta}^2\lvert\overline{S}\rvert\overline{S}_{ij}$
DTMM	$-2c_{m1}\overline{\Delta}^2\lvert\overline{S}\rvert\overline{S}_{ij} + c_{m2}\left(L_{ij} - \frac{\delta_{ij}}{3}L_{kk}\right)$
SDC1[b]	$\left(\phi_{ij} - \frac{\delta_{ij}}{3}\phi_{kk}\right) + \left(N_{ij} - \frac{\delta_{ij}}{3}N_{kk}\right)$
SDC2	$\left(\phi_{ij} - \frac{\delta_{ij}}{3}\phi_{kk}\right) + c_1\left(N_{ij} - \frac{\delta_{ij}}{3}N_{kk}\right)$
DC	$\left(L_{ij} - \frac{\delta_{ij}}{3}L_{kk}\right) + c_2\left(\mathfrak{R}_{ij} - \frac{\delta_{ij}}{3}\mathfrak{R}_{kk}\right)$

[a] The coefficients c_s, c_{m1}, c_{m2}, c_1 and c_2 are calculated dynamically.

[b] $N_{ij} = (\overline{\overline{w}_i\overline{v}_j} - \overline{\overline{w}}_i\overline{\overline{v}}_j + \overline{\overline{v}_i\overline{w}_j} - \overline{\overline{v}}_i\overline{\overline{w}}_j)$.

3. Simulations

To assess the performance of the proposed closures, they are employed for LES of the following flow configurations: (1) homogeneous isotropic (HI), (2) homogeneous shear (HS), and (3) temporally developing shear layers (TSLs). The assessment is primarily by means of comparison of the LES results with those obtained by DNS of these flows with the same magnitude of the physical parameters. All simulations (in both LES and DNS) consider unsteady, three-dimensional (3D) flows. The spatial discretization is by a spectral-collocation numerical scheme utilizing Fourier basis functions similar to that employed in our previous contributions (e.g. [22–24]). Time advancement is via the second-order Adams–Bashforth temporal discretization. The resolution in DNS is dictated by the magnitudes of the physical parameters, with vigorous testing of the independency of the results to the grid resolution. Simulations of the HI and the HS flows are conducted within a cubic box containing 128^3 collocation points. The resolution for DNS of the TSLs is 96^3. In all simulations, the grid spacing in all directions is uniform and equal.

For the homogeneous flows, triply periodic boundary conditions are employed. In the homogeneous shear flow a linear mean profile (with a normalized gradient of $S = 2$) along the transverse (y)-direction with grid transformation is employed. Also, in the homogeneous flows, the velocity field is initialized as a random solenoidal, three-dimensional field with a zero mean and Gaussian spectral density function. This initial field is allowed to evolve for a sufficient time to reach a "self-similar" state before LES is conducted. In mixing layer simulations, periodic boundary conditions along the streamwise (x)- and the spanwise (z)-directions and free slip boundary conditions along the cross-stream (y)-direction are imposed. To expedite the formation of large scale vortices, low amplitude forcing is initially superimposed on the mean flow. The flow field in this setting is dominated by large scale coherent structures. The length in streamwise direction is twice of the wavelength of the most unstable mode as given by the linear stability theory. This allows for the roll-up of the spanwise vorticity, resulting in two spanwise rollers at the non-dimensional time $t \approx 3$ followed by pairing of these vortices at $t \approx 6$. Two TSLs are considered. In TSL1 there are almost no initial 3D perturbations. In TSL2, an initial random solenoidal 3D velocity field with a zero mean and Gaussian spectrum is superimposed on the mean velocity field. The parameters in the four cases considered by DNS are summarized in Table 2 indicating the magnitude of the Reynolds number (Re_λ) based on the rms value of velocity fluctuations ($u_{\rm rms} = \sqrt{1/3\langle u_i u_i\rangle}$) and the Taylor micro-scale (λ), the Kolmogorov length scale (η) and the initial rms of the velocity fluctuations.

Table 2
The specifications of DNS cases

Case #	Flow type	Re_λ[a]	$\eta k_{\max}$[a]	$(u_{\rm rms})_{t=0}$[b]
1	HI	78.8–29.3	1.1–2.2	0.9
2	HS	34.7–65.8	1.2–1.1	0.65
3	TSL1	–	–	≈ 0
4	TSL2	–	–	0.01

[a] The values at the starting and ending times.

[b] For the HI and the HS flows this is the initial *rms* of the velocity fluctuations. For TSL1 and TSL2 this is the rms of the initial random perturbations added to the mean.

The LES results are dependent on the filter function and filter size. Here we only use the convolved box filter in the physical space. This filter provides the necessary overlap between the resolved and the subgrid stresses and yields results qualitatively similar to those with the Gaussian filter [9]. The sharp spectral cutoff filter does not allow an overlap range between the resolved and SGSs, and with its use some of the interesting properties of the models considered here would vanish [13]. Both "exact" and "approximate" versions of the box filter at the grid- and the test-levels are employed. The exact filter is used to calculate the "true" subgrid values and is invoked by averaging over fine (DNS) grid points. The approximate filter is performed over coarse (LES) grid points. The 3D approximate filter operator is split into 1D operations along each direction to reduce the computational time [19]. This splitting results in negligible errors at high wavenumbers of the resolved field. The filter size is selected by a compromise between the accuracy and the computational cost. Here, the characteristic length scale of filter at the grid-level ($\overline{\Delta}$) is twice the grid spacing in LES ($(\delta x)_{\rm LES}$) to minimize the relative effects of numerical discretization [25,26]. The filter size at the test-level ($\widehat{\Delta}$) is twice that at the grid-level (i.e. $\widehat{\Delta}/\overline{\Delta} = 2$) as suggested in previous studies [10]. The resolution in LES is specified by the ratio of the filter size at the grid-level to the grid spacing in DNS ($\mathscr{R} = \overline{\Delta}/(\delta x)_{\rm DNS}$). For example, with 128^3 collocation points in DNS and with $\mathscr{R} = 8$ the resolution in LES would be 32^3. Four approximate box filters are considered (Table 3). In the first (*FILT*#1), $\mathscr{R} = 8$ and the filtered values are evaluated by the trapezoidal rule [19, 26]. The second (*FILT*#2) and the third (*FILT*#3) filter functions are similar to the first but with $\mathscr{R} = 12$ and $\mathscr{R} = 16$, respectively. In the fourth (*FILT*#4), the filter size is the same as that in *FILT*#1 but the filtered values are evaluated by averaging of the grid values with an equal weight. In the presentations below *FILT*#1 is used for homogeneous simulations and *FILT*#2 is used for mixing layer simulations unless otherwise indicated.

Table 3
The time averaged correlation coefficient between L_{12} and L_{12}^*

Filter	$\overline{\Delta}/(\delta x)_{\mathrm{DNS}}$	Filter approximation	HI	HS	TSL2
FILT#1	8	Trapezoidal	0.996	0.996	0.997
FILT#2	12	Trapezoidal	–	–	0.973
FILT#3	16	Trapezoidal	0.953	0.941	–
FILT#4	8	Equal-weighting	0.990	0.991	0.992

The LES results of HI flow indicate that as simulations proceed the very high wavenumber values of the resolved velocity spectrum gradually exceed the corresponding values calculated from DNS data. Although this does not lead to numerical instabilities when SDC2 and DC are used, it does decrease the overall accuracy. By setting the filter size to twice the grid size, the resolved field is smoother and contains progressively less information about the small scales. This could decrease the accuracy of the proposed SGS models in that they cannot accurately predict the SGS stresses at the resolved scales below the characteristic scale of the filter (subfilter scales). Moreover, the models are unable to account for the nonlocal interactions at the smallest scales of the resolved field which are expected to have dissipative nature. To resolve this problem, in all a posteriori assessments, it is required to enforce a net dissipative effect on the subfilter scales of the resolved field. This is enacted here via the following procedure: first, the subfilter value of ϵ (denoted by ϵ'') is evaluated by a box filter with a characteristic size half of that at the grid-level (the size of filter is controlled by the weights of the grid point values in the filtering operation). Then, at each grid point, either the negative values of ϵ'' are eliminated, or an equivalent diffusivity is added. To eliminate the negative values, the Smagorinsky model is added (only at the grid points with negative ϵ'' values) to the modeled stresses to induce an equivalent positive dissipation. Alternatively, an equivalent diffusivity is added by modification of the molecular diffusivity coefficient in such a way as to cancel the negative values of ϵ''. Both of the above numerical procedures yield very similar results. This numerical procedure causes some small discontinuity in the stress field much less than that obtained when negative diffusivity (backscatter) is eliminated all together. As shown below, this procedure does not have a significant effect on the accuracy of SGS stresses.

4. Results and discussions

The comparison between the LES and the DNS results is made by means of both a priori and a posteriori analyses. In the former, DNS data are used to calculate both the true and the modeled values of SGS stresses. In the latter, the statistics of the resolved field as predicted by LES are compared with those obtained directly from DNS. The models are tested in a localized manner without averaging over homogeneous directions. Statistical analysis of data are conducted by averaging over the homogeneous directions. For the HI and the HS flows the temporal evolution of the volumetric averaged statistics are of primary importance and are presented. For the TSLs the averaging are conducted over x–z planes (represented by [ ]) and the y-dependent statistics are considered. In some cases the volumetric averaged statistics for the TSLs are also reported. The primary statistical quantities considered below are the correlation coefficient between variables A and B, $\rho(A,B)$ and the probability density function (PDF) of the statistical quantities.

4.1. A priori analysis

To assess the accuracy of the models, the correlation coefficient between the DNS and the modeled values of SGS stresses for different flows are considered in Fig. 1. In the results shown in this figure and those shown below the "time" t^* is the time normalized by the final time of the simulation in each case and $\rho(\underline{\alpha},\underline{\beta}) = (\rho(\alpha_{12},\beta_{12}) + \rho(\alpha_{13},\beta_{13}) + \rho(\alpha_{23},\beta_{23}))/3$ where $\underline{\alpha}$ and $\underline{\beta}$ are second order tensors. In the HI flow, after the transient time, the correlation coefficients for all models increase slightly with the decay of turbulence. In the HS and the TSL2, the correlation coefficients do not vary significantly in time. Fig. 1 indicates that DTMM performs better than DSM and the newly proposed closures perform better than DTMM in all cases. In SDC2 and DC the spatial variations of the constants (c_1, c_2) are considerably lower than those in the model constant of DSM and DTMM (not shown). Fig. 1 also shows that the correlation coefficients between DNS and SDC2* values of SGS stress are considerably lower than those between DNS and SDC2. This is due to significant difference of the local model (SDC2*) coefficients at the grid- and the test-level.

A more vigorous testing of the models is conducted in Fig. 2, where the PDFs of exact and modeled values of τ_{12} in the HS flow are considered. Consistent with the results in Fig. 1, it is observed that the PDF of τ_{12} as predicted by DSM is noticeably different from that of

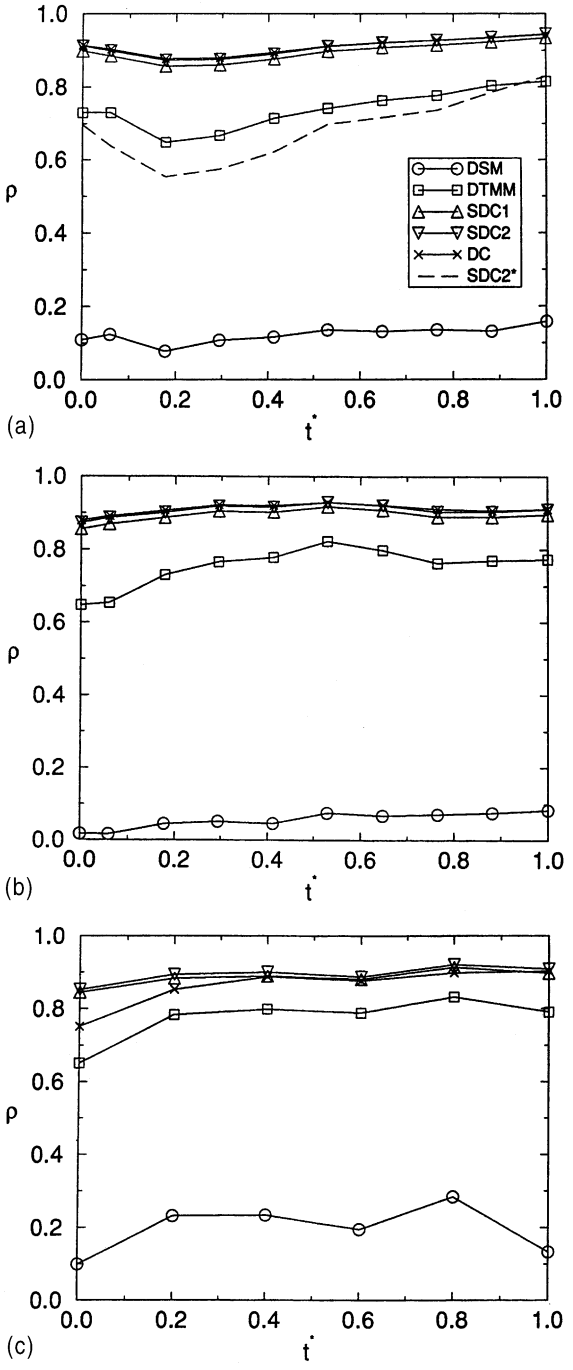

Fig. 1. Temporal variations of the correlation coefficient between the DNS and modeled values of the SGS stresses, $\underline{\tau}$ in (a) HI, (b) HS, and (c) TSL2.

DNS. The PDF predicted by DTMM is closer to the true PDF but does overpredict the positive (and somewhat negative) stress values. The ability of SDC1, SDC2 and DC to predict the true subgrid stress is evident. The

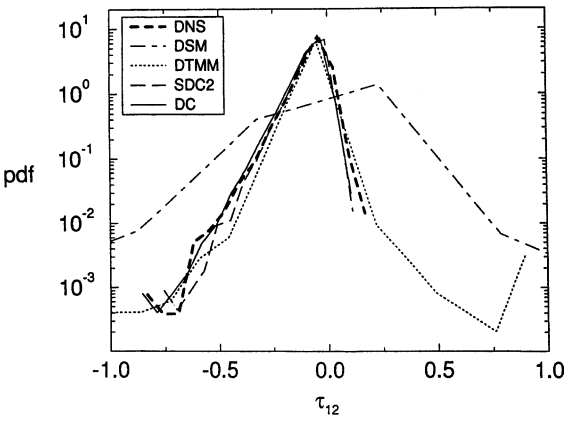

Fig. 2. The PDFs of τ_{12} in the HS flow at $t^* = 0.11$.

results for other SGS stresses at different times, and for other flows exhibit a similar behavior.

One of the most important requirements of the SGS model is to correctly predict the energy transfer from the resolved field to the subgrid field. One can consider the energy transfer as the effects of very small-scale eddies on the resolved scales across a "spectral-gap" (nonlocal effects) combined with the effects of intermediate-size eddies which constitute the spectral-gap (local effects). The nonlocal effects can be approximated by a positive eddy diffusivity if the spectral-gap is sufficiently large. It is unlikely that stochastic and gradient diffusion type models properly represent the local effects. In SDC1, SDC2 and DC the effects of intermediate-size eddies on the resolved scales are explicitly evaluated from the dynamics of the resolved field. Therefore, these models are expected to predict the energy exchange between the resolved and SGSs with reasonable accuracy. To demonstrate this, in Table 4, the time averaged values of the correlation coefficient between the true and the modeled values of ϵ and the rms values of ϵ at $t^* = 2.2$ for the HI flow are shown. The results for the HS and the TSL exhibit similar trends. The results in Table 4 are in accord with those in Figs. 1 and 2, indicating that the dissipation values predicted by DSM correlate poorly with the true values. The ability of DTMM to predict the correct SGS dissipation is better than DSM but considerably less than SDC1, SDC2 and DC.

A reason that the proposed closures accurately predict the SGS stresses is that they treat the substresses, **L**, **C** and **R** separately. These substresses each contribute significantly to the total SGS stress. This is demonstrated in Fig. 3, where the temporal variations of the percentage of the Leonard (L_{12}), cross (C_{12}) and Reynolds (R_{12}) parts of the τ_{12} stress are shown. The results in this figure are obtained by filtering the DNS data over fine grids with two different filter sizes. To calculate the contribution of L_{12}, C_{12} and R_{12}, the absolute values of

Table 4
The correlation coefficient and the rms of SGS dissipation

Quantity	DNS	DSM	DTMM	SDC1	SDC2	DC	SDC2*
ρ	1.0	0.373	0.584	0.871	0.887	0.892	0.712
Rms at $t^* = 0.22$	0.037	0.061	0.034	0.031	0.036	0.039	0.035

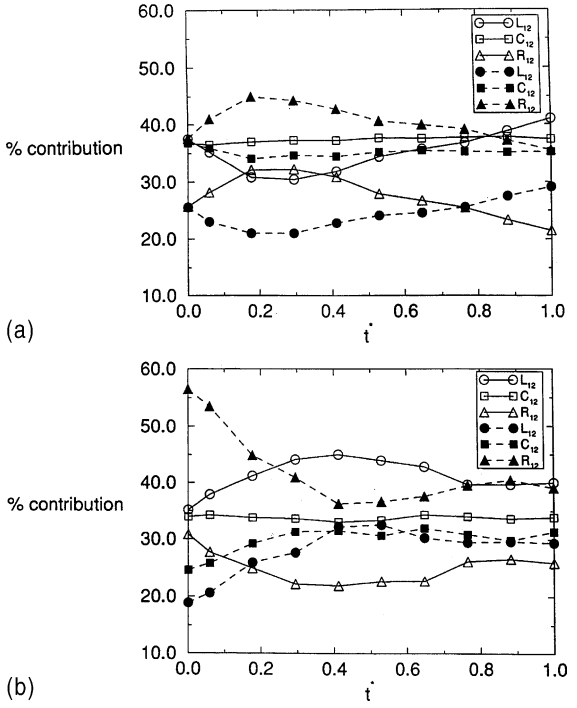

Fig. 3. Temporal variations of the percentage of L_{12}, C_{12} and R_{12} in (a) HI, and (b) HS. The solid lines with hollow symbols refer to *FILT*#1 and the dashed lines with filled symbols refer to *FILT*#3.

these quantities are considered. For example the percentage of the contribution of the Leonard term is equal to $100 \times [|L_{12}|/(|L_{12}| + |C_{12}| + |R_{12}|)]$. The results in Fig. 3 indicate that in both the HI and the HS flows L_{12}, C_{12} and R_{12} each have a significant contribution. However, as the filter size increases the relative magnitude of L_{12} decreases and those of R_{12} and τ_{12} increase. The percentage of C_{12} does not vary significantly with the filter size. In the HI flow (Fig. 3(a)), with the decay of turbulence the contribution of R_{12} gradually decreases and that of L_{12} increases. The reason is that a significant part of the Reynolds term is due to nonlocal effects of SGS on the resolved field. With the decay of energy at smallest scales of SGS the nonlocal effects become less significant and the percentage of R_{12} decreases. In the HS flow (Fig. 3(b)), after the initial transient time, the statistical behavior of SGS and therefore the contributions of the Reynolds and the Leonard terms do not vary significantly in time. In the TSL1, the flow is dominated with large scale two dimensional vortical structures. It is therefore expected that the Leonard and cross terms contribute significantly to the total SGS stress. Our results (not shown) indicate that for TSL1 more than 80% of τ_{12} is due to L_{12} and C_{12}. The relative importance of the Reynolds term, however, increases as the flow becomes more three-dimensional. In TSL2 (with three-dimensional random initial perturbations) the relative amount of R_{12} is much more significant than that in TSL1. It is to be noted that in TSL1 the flow remains two-dimensional with small variations along spanwise direction. In TSL2, the flow exhibits significant three dimensionality, particularly at SGSs. In the discussion below, only the results for the HI, the HS and the TSL2 flows are presented.

The PDFs of the L_{12}, C_{12} and R_{12} are shown in Fig. 4. In HI flow (Fig. 4(a)), the PDFs of the three stresses are similar. In HS flow (Fig. 4(b)) the PDF of L_{12} is highly skewed toward negative values. The PDFs of C_{12} and R_{12} are more symmetric because the smaller scales of turbulent fluctuations in this anisotropic flow exhibit a higher degree of local isotropy. Also shown in Fig. 4 are the PDFs of L^*_{12} calculated from DNS data over coarse (LES) grids with *FILT*#1. In the LES models of Zang et al. [19] and Salvetti and Banerjee [12] the Leonard term is calculated explicitly and is assumed to be identical to "exact" values. These exact values are denoted by L_{ij} and are obtained by using the DNS data over fine grids. The approximate values are obtained by applying *FILT*#1 to DNS data over coarse grids and are denoted by L^*_{ij}. In a priori analysis the model should be evaluated solely based on information available over coarse (LES) grid points. The results in Fig. 4 and those in Table 3 indicate that the difference between L_{ij} and L^*_{ij} is indeed very small, as for all filters listed in Table 3 the time averaged values of $\rho(L_{12}, L^*_{12})$ are close to unity. The values of $\rho(L_{12}, L^*_{12})$ decreases slightly as the filter size increases and/or when L^*_{12} is calculated with *FILT*#4. Based on these results, it is concluded that the local values of the Leonard term, calculated over coarse grids (L^*_{ij}) represent the true values (L_{ij}) with very good approximation. Hereinafter the star superscript is dropped.

To further explain the results in Figs. 1–4, the time averaged values of the correlation coefficients between several subgrid quantities are considered in Table 5. In

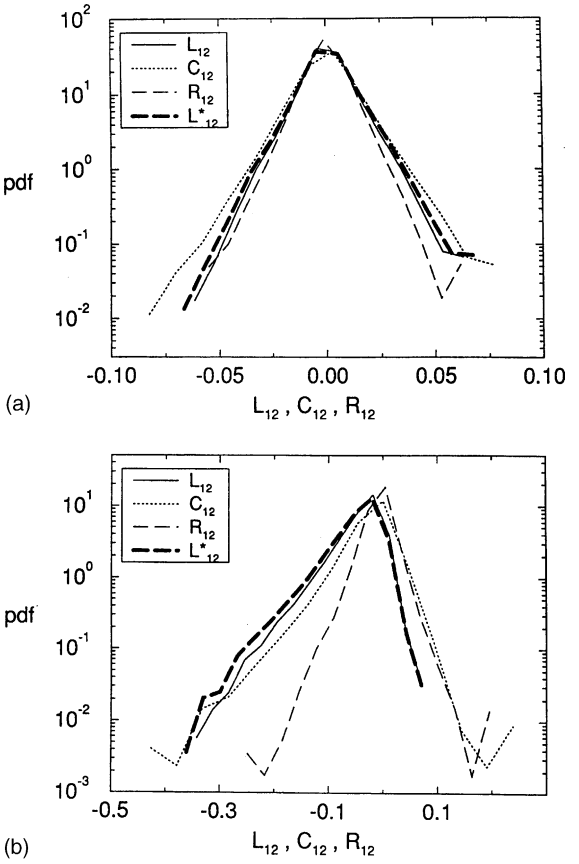

Fig. 4. The PDFs of L_{12}, L^*_{12}, C_{12} and R_{12} in (a) homogeneous isotropic, (b) homogeneous shear, flows.

Table 5
The time averaged correlation coefficient between different quantities

Correlation coefficient	HI[a]	HS	TSL2
$\rho(\underline{\tau},\underline{\Gamma})$	$0.27^{+0.02}_{-0.02}$	$0.19^{+0.03}_{-0.05}$	$0.26^{+0.06}_{-0.1}$
$\rho(\underline{T},\underline{\Gamma}^{\mathrm{T}})$	$0.32^{+0.04}_{-0.05}$	$0.17^{+0.13}_{-0.11}$	$0.71^{+0.08}_{-0.09}$
$\rho(\underline{\tau},\underline{L})$	$0.82^{+0.04}_{-0.05}$	$0.82^{+0.03}_{-0.05}$	$0.81^{+0.04}_{-0.04}$
$\rho(\underline{T},\underline{L}^{\mathrm{T}})$	$0.94^{+0.02}_{-0.02}$	$0.94^{+0.02}_{-0.02}$	$0.96^{+0.02}_{-0.01}$
$\rho(\underline{\xi},\underline{\mathfrak{R}})$	$0.81^{+0.02}_{-0.02}$	–	–
$\rho(\underline{\xi},\underline{L})$	$0.59^{+0.04}_{-0.05}$	–	–
$\rho(\tau_{12},\tau^*_{12})$	$0.997^{+0.000}_{-0.000}$	$0.996^{+0.000}_{-0.000}$	$0.996^{+0.001}_{-0.001}$
$\rho((\psi_{12})_{\mathrm{DNS}},(\psi_{12})_{\mathrm{SDC2}})$	$0.65^{+0.04}_{-0.04}$	–	–
$\rho((\psi_{12})^*_{\mathrm{DNS}},(\psi_{12})_{\mathrm{SDC2}})$	$0.55^{+0.02}_{-0.04}$	–	–

[a] The upper and the lower values with plus and minus sign represent the deviation of maximum and minimum values respectively from the averaged quantity.

this table, $\underline{\Gamma} \equiv \overline{\Delta}^2|\overline{S}|\overline{S}_{ij}$ and $\underline{\Gamma}^{\mathrm{T}} \equiv \widehat{\overline{\Delta}}^2|\widehat{\overline{S}}|\widehat{\overline{S}}_{ij}$ represent the Smagorinsky closure at the grid- and the test-levels, respectively. The results in Table 5 indicate that $\rho(\underline{\tau},\underline{\Gamma})$ is much smaller than $\rho(\underline{\tau},\underline{L})$. This is in accordance with previous observations [7,9] and indicates that the "scale-similarity" type closures are potentially more accurate than the "eddy diffusivity" type closures. It is interesting that the correlation coefficients do not dependent significantly on the flow configuration. At the test-level, the correlation coefficients between the SGS stress and its Leonard part are also similar and exhibit higher values compared to those at the grid-level. For the HI and the HS flows, there is a relatively poor correlation between the true SGS stresses and those obtained from the Smagorinsky model. However, in the TSL, the ability of the Smagorinsky closure to predict the local values of SGS stress at the test-level is much better than that at the grid-level. In the HI and the HS flows the anisotropic elements of the SGS stress tensor are almost equally important. In the TSL τ_{12} is significantly larger than τ_{13} and τ_{23}. Also, $\rho(\tau_{12},L_{12})$ is larger than $\rho(\tau_{13},L_{13})$ and $\rho(\tau_{23},L_{23})$ because the flow is dominated by large scale structures in the x–y plane.

The accuracy of the dynamic models improves as more accurate base closures are used to model the SGS stresses at the grid- and test-levels. Based on the results in Table 3, it is clear that the Leonard part of SGS stress could be accurately evaluated by using the data available over coarse grids. Additionally, the results shown in Table 5 indicate that regardless of flow configuration, the correlation between the remaining part of SGS stress, $\xi_{ij} = C_{ij} + R_{ij}$ and $\mathfrak{R}_{ij}$ is considerably higher than that between ξ_{ij} and L^*_{ij}. It is not, therefore, surprising that DC and SDC2 predict the local values of SGS stresses better than DSM and DTMM.

The SDC closures are developed based on decomposition of the Leonard, cross and Reynolds components of the SGS stresses into sequential "Leonard", "cross" and "Reynolds" terms of their own. However, this SDC can be extended further. To assess the convergence properties of the SDC, in Fig. 5 the DNS generated PDFs of the SGS stresses in the HI flow as obtained by truncation of the decompositions at three different levels are shown. At the first and the second levels, the stresses are equivalent to those corresponding to L_{ij} and SDC1, respectively. At the third level, ψ_{ij} in Eq. (8) is decomposed similar to τ_{ij} at the second level. Expectedly, it is observed that with increasing the order of truncation, the predicted PDFs become closer to the "exact" PDF as more significant parts of the stress are accounted for explicitly. The stresses obtained by the first level truncation are significantly different than the exact values. The predicted results improve significantly by increasing the truncation to the second level. But the extent of improvement is not as much by advancing to the third level. Our results also indicate that the time averaged correlation coefficients between the exact values of τ_{12} and those predicted by decomposition at levels 1–3 are 0.807, 0.894 and 0.911, respectively. As indicated before, the truncation level can be increased

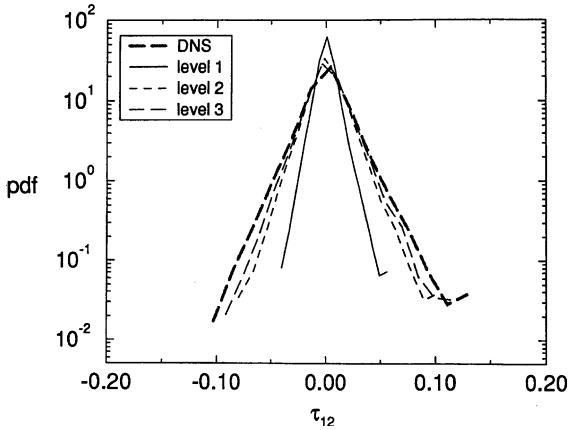

Fig. 5. The PDFs of the DNS and modeled values of τ_{12} in the HI flow.

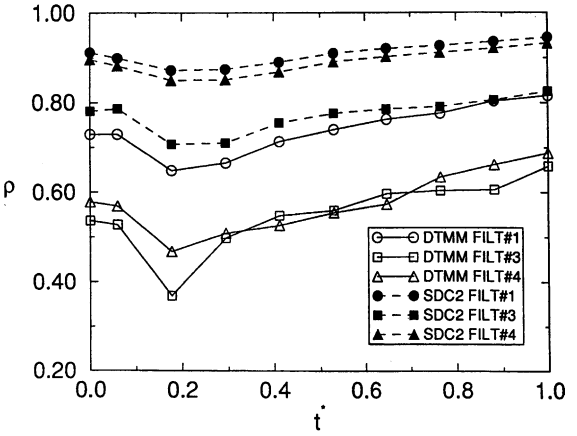

Fig. 6. Temporal variations of the correlation coefficient between the predicted values of $\underline{\tau}$ by SDC2 and DTMM in the HI flow.

further, with the obvious penalty of higher computational cost. Based on these results, the truncation at the second level is implemented in SDC closures (SDC1 and SDC2).

While the performance of the stress models improve as more significant portions of the SGS stresses are explicitly evaluated, the filtering operation over the coarse grids is not error free. Therefore, the accuracy of the SGS stress models must be assessed. This is considered in Table 5 where the correlation coefficients between τ_{12} and τ^*_{12} for different flows are considered. In the evaluation of τ^*_{ij} the "resolved" part (ϕ_{ij} in Eq. (8)) is calculated explicitly based on the information available over coarse grids while in the evaluation of τ_{ij} the information over fine (DNS) grids is employed. It is observed that for all flow configurations, $\rho(\tau_{12}, \tau^*_{12})$ is very close to unity at all times. We also found that $\rho(\tau_{12}, \tau^*_{12})$ decreases slightly as the size of filter is increased. For example, the time averaged value of $\rho(\tau_{12}, \tau^*_{12})$ for the HS flow decreases from 0.996 to 0.974 as the filter size is doubled.

The very high correlations between τ_{12} and τ^*_{12} indicate that ϕ_{ij} is accurately calculated from the information available over the coarse grids. Thus the performance of SDC closures can be significantly improved by using more accurate models for ψ_{ij}. The correlation coefficients between $(\psi_{12})_{\mathrm{DNS}}$ and $(\psi_{12})_{\mathrm{SDC2}}$ and those between $(\psi_{12})^*_{\mathrm{DNS}} = (\tau_{12})_{\mathrm{DNS}} - (\phi_{12})_{\mathrm{LES}}$ and $(\psi_{12})_{\mathrm{SDC2}}$ are shown in the last two rows in Table 5. The results for both the HI and the HS flows are similar and indicate a moderate correlation between DNS and modeled values. It is, however, observed that $\rho[(\psi_{12})^*_{\mathrm{DNS}}, (\psi_{12})_{\mathrm{SDC2}}]$ is significantly higher than $\rho[(\psi_{12})_{\mathrm{DNS}}, (\psi_{12})_{\mathrm{SDC2}}]$. This is because the coarse grid filter function is only an approximation of the exact filter function and some information is lost. This issue is also addressed by Zhou et al. [27] in a different context.

In Fig. 6 the effect of the filter size on the correlation coefficient between the exact and the modeled values of τ_{ij} is shown. For clarity, only the results for DTMM and SDC2 are considered. Expectedly, with increasing the filter size the correlations for both models decrease. However, the accuracy of SDC2 decreases less than that of DTMM as the size of the filter increases. It should be mentioned that for the range of Reynolds numbers considered, the filter size is close to the characteristic size of the energy containing scales. The performance of the proposed models is expected to be less sensitive to the filter size when the characteristic size of the filter is within the inertial range of high Reynolds number turbulence. The correlation between the modeled and the exact stress values is also dependent on the approximations made to evaluate the filtered variables over coarse grids. This is observed in Fig. 6, where it is shown that with changing filter function from *FILT*#1 to *FILT*#4 the correlation coefficients between the true stresses and those predicted by DTMM decrease significantly. There is not, however, a significant variation in the correlation coefficients between the true and SDC2 predicted values of SGS stresses.

To further assess the dependency of the models to the filter, the correlation coefficients between DNS and the modeled values of SGS dissipation $\rho(\epsilon_{\mathrm{DNS}}, \epsilon_{\mathrm{model}})$, for various filters are calculated. Υ_3 is the percentage of the difference between $\rho(\epsilon_{\mathrm{DNS}}, \epsilon_{\mathrm{model}})$ evaluated by *FILT*#3 and that calculated by *FILT*#1, and Υ_4 is the percentage of the difference between $\rho(\epsilon_{\mathrm{DNS}}, \epsilon_{\mathrm{model}})$ evaluated by *FILT*#4 and that calculated by *FILT*#1. In Table 6, time averaged values of Υ_3 and Υ_4 for different models and in the HI and the HS flows are considered. The results are consistent with those in Fig. 6, indicating that the capability of DSM and DTMM to predict ϵ is strongly dependent on the size of the filter as well as the ap-

Table 6
The time averaged values of Υ_3 and Υ_4

Variable	Flow	DSM	DTMM	SDC1	SDC2	DC
Υ_3	HI	30.1	34.0	19.5	17.7	18.8
Υ_3	HS	81.2	48.4	14.2	13.5	14.9
Υ_4	HI	37.9	34.8	1.9	1.5	2.1
Υ_4	HS	62.6	32.4	1.7	1.3	2.0

proximation made in the discrete representation of the filter function over the coarse grids. The performances of other models (SDC1, SDC2 and DC) are much less sensitive to the filter parameters.

4.2. A posteriori analysis

Even with a very accurate SGS closure, the statistical uncertainty and the numerical errors can cause gradual decorrelation of LES and DNS results. This "secular" behavior (or lack thereof) is an important issue and its assessment requires a posteriori analysis.

As discussed in Section 3, to ensure the numerical stability and to increase the accuracy of the models in a posteriori assessments the backscatter of energy predicted by all models at "subfilter" scales is removed. To understand how the elimination of "subfilter" backscatter affects the accuracy of the models, priori tests are conducted in which the SGS stresses with and without the subfilter backscatter are compared. Sample results are shown in Fig. 7 for the HI flow, in which the suffix "clipped" denote the cases in which the subfilter backscatter is eliminated. It is observed in Fig. 7 that the PDFs of SGS dissipation obtained by DNS and DC are not significantly affected when the backscatter at subfilter level is removed. We have also found that the correlation between DNS and DC values of the SGS stress is not affected when the subfilter backscatter is removed. This is not, however, the case for DSM as the performance of this model improves slightly when the predicted subfilter backscatter is eliminated. With this assessment, a posteriori simulations are conducted of all three flow configurations, the results of which are discussed in order.

4.2.1. Homogeneous isotropic flow

In consideration of this flow by LES, the simulations without a subgrid model and those with DSM and DTMM failed due to numerical instabilities. Therefore, these two models are implemented in a localized manner [19,20] by local averaging over the test filter domain, and by clipping of the negative eddy viscosity values. Fig. 8

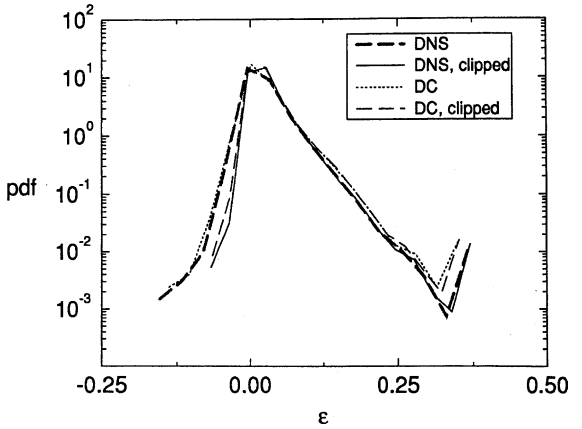

Fig. 7. The PDFs of the DNS and modeled values of τ_{12} in the HI flow.

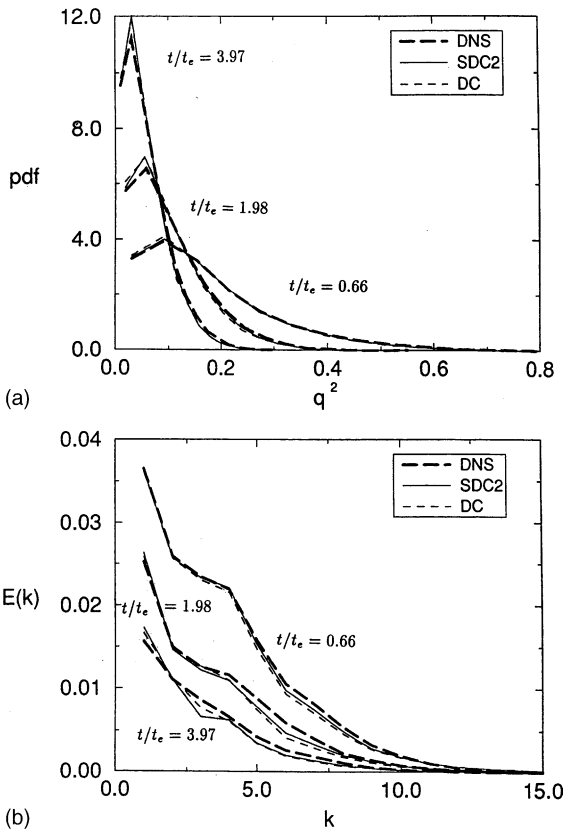

Fig. 8. Statistics of the resolved field in the HI flow: (a) the PDFs of the energy, (b) the spectral density function.

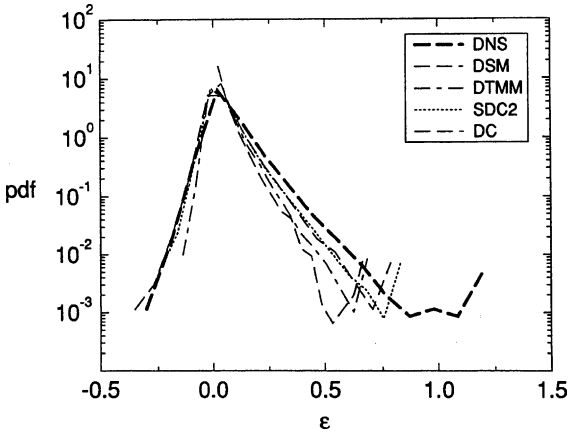

Fig. 9. The PDFs of SGS dissipation in the HI flow at $t/t_e = 0.66$.

shows that the PDFs of the resolved field energy ($\bar{q}^2 = (1/2)\overline{u}_i\overline{u}_i$) and the three-dimensional spectral density functions of the resolved velocity field ($E(k)$) are also predicted well by LES at all times. A comparison between the PDFs of τ_{12}, calculated from DNS and LES, indicates that the PDFs predicted via SDC2 and DC are close to those obtained from DNS data with only a slight underprediction of high stress values. The DSM predictions deviate significantly from DNS, and the accuracy of DTMM is between that of DSM and the new proposed models. These results are consistent with the results of a priori analysis.

The PDFs of ϵ as obtained by DNS and those predicted by the models are shown in Fig. 9. The DNS results indicate that the PDF of ϵ is significantly skewed toward positive values indicating a net (volumetric averaged) dissipative effect of SGS on the resolved scales. There is, however, a significant backscatter which is not accounted by DSM. The results for ϵ in Fig. 9 are consistent with those for τ_{12} in that the accuracy of DTMM is between those of DSM and the new proposed models. Fig. 9 also demonstrates that the energy transfer (both forward and backward) from SGS to the large scales is predicted reasonably well by SDC2 and DC. However, these models underpredict the high positive values of ϵ. These high stress values mostly occur at the smallest scales of the resolved field and are highly intermittent.

4.2.2. Homogeneous shear flow

The results for the HI flow demonstrate that the proposed models cannot fully account for the nonlocal and dissipative effects of SGS motions at the smallest scales of the resolved field. This is partially due to the size of the filter. With increasing the filter size, the numerical errors become relatively smaller but the accuracy of the model to predict the interactions at smallest scales of the resolved field (those with typical size less than the filter size) is reduced. Also, the models do not account for finite Reynolds number effects which are expected to be noticeable in our simulations.

The model inaccuracies and the numerical errors are expected to result in more significant differences between the DNS and the LES results at long times in the HS flow as compared to the HI flow. This is due to the fact that in the HS flow the SGS stresses contribute to both dissipation and production of energy. In Fig. 10(a), the growth of the variance ($2\bar{q}^2$) as predicted by the models is compared with that obtained by DNS. The simulations without a SGS closure were unstable. Also, LES with DSM, DTMM become unstable if negative values of c_1 and c_2 are retained. Therefore, similar to that in the HI flow, these models are implemented with local averaging of c_1 and c_2 and clipping of their negative values. A modified version of DC (termed "DCp") is also considered. This model is similar to DC except that the model coefficient (c_2) is evaluated by the procedure suggested by Piomelli and Liu [20]. Fig. 10(a) shows that

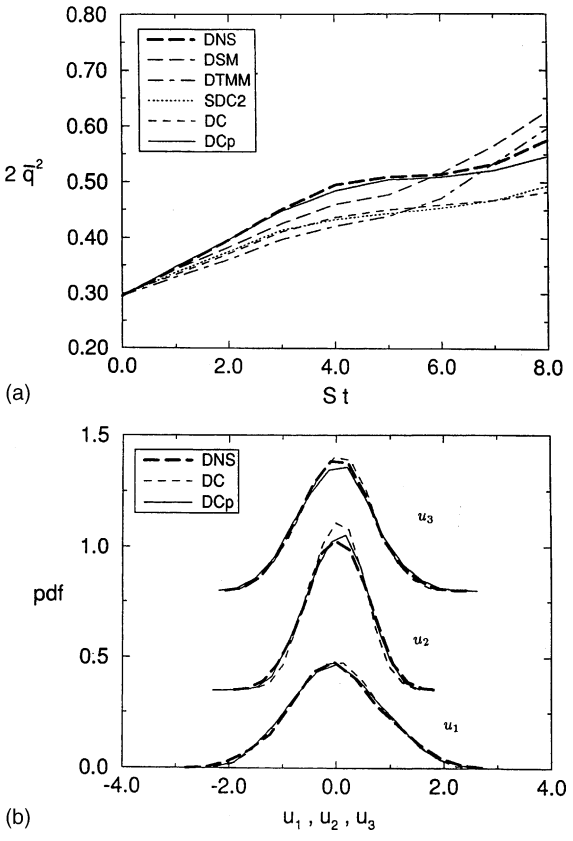

Fig. 10. (a) Temporal variations of the variance of the resolved field velocity in the HS flow, (b) The PDFs of the velocity components in the HS flow at $St = 4$, the curves for u_2 and u_3 are shifted upwards for clarity.

at short times, SDC2 and DC predict the growth of the energy reasonably well. However, the errors become increasingly significant at later times. For $St < 5.5$, the growth of energy is significantly underpredicted when DTMM is utilized. For $St > 5.5$, a rapid growth in energy is predicted by DTMM which is not in accordance with DNS results. In contrast to that observed for the HI flow, the performance of DSM is better than DTMM. The LES predictions obtained by DCp are close to DNS results at all times. The DNS and LES generated PDFs of ϵ in the HS flow exhibit a behavior similar to that shown in Fig. 9.

There is some evidence that the anisotropy at large scales may be correlated to the anisotropy at small scales. It is therefore unlikely that the anisotropy of the resolved field can be accurately captured by LES if the subgrid models cannot account for the anisotropy in the SGS stress tensor. Models such as those proposed above are capable of capturing the anisotropic nature of SGS motions. In Fig. 10(b) it is shown that even at $St = 4$, the PDFs of all velocity components as predicted by DC and DCp are very close to those obtained by DNS. The most significant difference is observed for the velocity component along the mean shear direction (u_2). The results in Fig. 10(b) demonstrate that despite its limitations, DC successfully predicts the local and averaged quantities in the HS flow for a relatively long time. The results obtained with SDC1 and SDC2 are similar to those shown for DC.

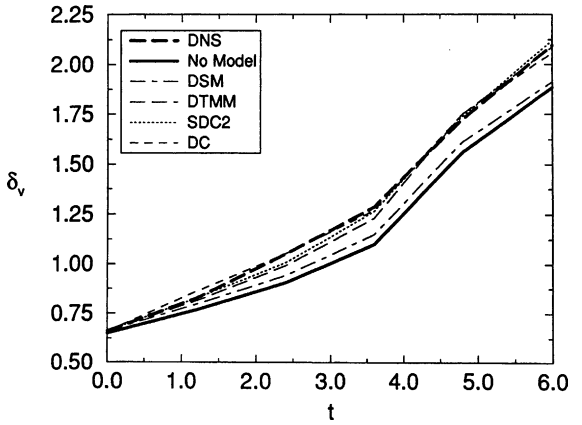

Fig. 11. Temporal variations of the vorticity thickness in TSL2.

4.2.3. Temporal shear layer flow

The primary dynamics in inhomogeneous shear flow are associated with large scale structures with forward and reverse energy exchange with the fine scales. Accurate modeling of this energy exchange is essential for accurate predictions of the flow development. The results of a priori analysis indicate that the models developed here capture both the forward and the backward energy transfer between the SGS and the resolved scales correctly. It is, therefore, expected that the growth of the shear layer is predicted well via these models. This is confirmed in Fig. 11, where the temporal evolution of the vorticity thickness (δ_v) in TSL2 is shown. Without a subgrid model, the simulations at this moderate Reynolds number are stable but the growth of the layer is significantly underpredicted. The results predicted by DTMM, SDC2, DC and DCp exhibit the best overall agreement with DNS data. The relative success of the LES in reproducing the filtered DNS data is due to the ability of the proposed models to correctly represent the local values of the SGS energy dissipation. Our results (not shown) indicate that despite small deviations at high dissipation values, the true SGS dissipation is accurately predicted by the proposed models in TSL2.

Computational requirements: For a comparative assessment, the computational times required for LES of homogeneous isotropic flow as conducted with various models are compared in Table 7. It is shown that the running time for LES with DSM is significantly larger than that required for implementation of the Smagorinsky closure. The time required for SDC1 is only slightly larger than that for DSM. The simulation times of DTMM, DC and SDC2 are somewhat equivalent; SDC2 is slightly more expensive than the others. Considering the improved accuracy of the new closures, the overhead associated with their computational implementation appears tolerable.

5. Concluding remarks

Localized SGS stress models are presented for use in LES of turbulent flows. The new models are constructed based on two different closure strategies. The first, termed the SDC model, is based on decomposition of the generalized Leonard (**L**), cross (**C**) and Reynolds (**R**) components of the SGS stresses into sequential "Leonard", "cross" and "Reynolds" terms of their own.

Table 7
The computational times for LES with various SGS stress models

Model	Smagorinsky	DSM	DTMM	SDC1	SDC2	DC
Normalized CPU time	1[a]	1.31	1.58	1.36	1.77	1.56

[a] Unit correspond to 128 seconds on a Cray-C90 computer which is the running time for 960 iterations of LES with 32^3 grid points.

The unclosed components of those sequential terms are modeled. The second, referred to as the DC closure, is based on the assumption that the local values of $\mathbf{C}+\mathbf{R}$ are highly correlated with the Leonard part of $\mathbf{R}$. Two forms of SDC (referred to as SDC1 and SDC2) and one form of DC are studied in detail here. The new proposed closures are applied "locally" and the predicted results are compared with those via the DSM of Germano et al. [10] and the DTMM of Salvetti and Banerjee [12]. The performance of the models is assessed via both a priori and a posteriori analyses by comparison with data obtained by DNS of homogeneous isotropic, homogeneous shear and inhomogeneous temporal shear layer flows.

The results of a priori analysis indicate that the new closures are more accurate than previously proposed closures, and are able to account for the anisotropy and transitional behavior of the SGS motions. The performance of SDC2 is similar to DC but it requires increased computational time. The advantage of SDC2 over DC is that it requires less modeling effort. The new proposed closures are also less sensitive to the filter size, as the accuracies of SDC1, SDC2 and DC decrease at a lower rate than those of DSM and DTMM when the filter size increases. Additionally, an improper approximation in coarse grid filtering operation influences the performances of SDC1, SDC2 and DC less than those of DSM and DTMM. The reasons for this better performance are (1) a significant part of SGS stresses is explicitly calculated, (2) the local interactions between the resolved and the SGS motions are well represented, and (3) the model coefficients do not vary significantly in space and are well correlated at the grid and the test-levels.

The results of a posteriori analysis indicate that in homogeneous isotropic flow, both the SGS stresses and the volumetric averaged statistics of the large scales are accurately predicted with the new closures. The performance of the proposed models in homogeneous shear flow is similar to that in homogeneous isotropic flow. However, the growth of the resolved field energy is underpredicted at long times. Simulations without a SGS stress model and also those with DSM or DTMM (applied in a localized manner) are unstable. This behavior is observed in both homogeneous isotropic and homogeneous shear flow; therefore, the coefficients in DSM and DTMM are calculated by local averaging over the test filter domain with clipping of the negative values. With this measure, the simulations become stable but the accuracy of the models is less than that of the new closures. In the temporal shear layer, LES with SDC2 and DC successfully predicts the layer's growth, the SGS stresses and other statistical quantities. The growth of energy in the homogeneous shear flow is better predicted when a modified version of DC (called DCp) is used. In SDC1 and SDC2, simple closures are used to model the remaining part of SGS stresses which are not calculated explicitly. The SDC models can be improved significantly by utilizing more accurate models for the unclosed parts.

Despite their demonstrated capabilities, there are some drawbacks associated with these closures. Our results show that SDC1, SDC2 and DC are not able to fully account for the effects of SGS motions on the smallest scales of the resolved field. This is partially due to the filter size which is twice the grid size, which limits the capability of the models to account for the nonlinear interactions at smallest scales of the resolved field. Additionally, the scale-similarity assumption as used to evaluate the model coefficients is questionable when there are significant nonlocal interactions between the subgrid and the resolved fields. These nonlocal interactions are expected to have random and dissipative effects on the resolved field. The important effects of the numerical discretization error should also be considered when DNS and LES results are compared. This issue is not addressed here and awaits further investigations.

Acknowledgements

This work is sponsored by the US Office of Naval Research under grant N00014-01-1-0843. Dr. Gabriel Roy is the Program Manager for this grant. Additional Support is provided by National Science Foundation under grant CTS0092665. Acknowledgments is also made to the Donors of the Petroleum Research Funds administered by the American Chemical Society for their support under grant ACS-PRF# 35676-G9. Computational resources are provided by the National Center for Supercomputer Applications (NCSA) at the University of Illinois at Urbana and by the San Diego Supercomputer Center.

References

[1] M. Ciofalo, Large Eddy Simulation: A Critical Survey of Models and Applications, in: Advances in Heat Transfer, vol. 25, Academic Press, New York, NY, 1994, pp. 321–419.

[2] D. Knight, L. Sakell (Eds.), Fluid Mechanics and its Applications, vol. 54, Kluwer Academic Publishers, The Netherlands, 1999.

[3] F.A. Jaberi, P.J. Colucci, Large eddy simulation of heat and mass transport in turbulent flows—Part 2: Scalar field, Int. J. Heat Mass Transfer, in press, (doi: 10.1016/S0017-9310(02)00485-4).

[4] J. Smagorinsky, General circulation experiments with the primitive equations. I. The basic experiment, Monthly Weather Rev. 91 (3) (1963) 99–164.

[5] P. Moin, J. Kim, Numerical investigation of turbulent channel flow, J. Fluid Mech. 118 (1982) 341–377.

[6] B. Galperin, S.A. Orszag (Eds.), Large Eddy Simulations of Complex Engineering and Geophysical Flows, Cambridge University Press, Cambridge, UK, 1993.
[7] J. Bardina, J.H. Ferziger, W.C. Reynolds, Improved turbulence models based on large eddy simulations of homogeneous, incompressible, turbulent flows, Department of Mechanical Engineering Report TF-19, Stanford University, Stanford, CA, 1983.
[8] U. Schumann, Stochastic backscatter of turbulence energy and scalar variance by random subgrid-scale fluxes, Proc. Roy. Soc. Lond. A 451 (1995) 293–318.
[9] S. Liu, C. Meneveau, J. Katz, On the properties of similarity subgrid-scale models as deduced from measurements in a turbulent jet, J. Fluid Mech. 275 (1994) 83–119.
[10] M. Germano, U. Piomelli, P. Moin, W.H. Cabot, A dynamic subgrid-scale eddy viscosity model, Phys. Fluids A 3 (7) (1991) 1760–1765.
[11] M. Germano, Turbulence: The filtering approach, J. Fluid Mech. 238 (1992) 325–336.
[12] M.V. Salvetti, S. Banerjee, A priori tests of a new dynamic subgrid-scale model for finite-difference large-eddy simulations, Phys. Fluids 7 (11) (1995) 2831–2847.
[13] S. Menon, P.K. Yeung, W.W. Kim, Effect of subgrid models on the computed interscale energy transfer in isotropic turbulence, Comput. Fluids 25 (2) (1996) 165–180.
[14] S. Ghosal, T.S. Lund, P. Moin, K. Akselvoll, A dynamic localization model for large eddy simulation of turbulent flows, J. Fluid Mech. 286 (1995) 229–255.
[15] M. Germano, A statistical formulation of dynamic model, Phys. Fluids 8 (2) (1996) 565–570.
[16] A.A. Aldama, in: Filtering Techniques for Turbulent Flow Simulations, Lecture Notes in Engineering, vol. 49, Springer-Verlag, New York, NY, 1990.
[17] R.M. Kerr, J.A. Domaradzki, G. Barbier, Small-scale properties of nonlinear interactions and subgrid-scale energy transfer in isotropic turbulence, Phys. Fluids 8 (1) (1996) 197–208.
[18] D.K. Lilly, A proposed modification of the Germano subgrid-scale closure method, Phys. Fluids A 4 (3) (1992) 633–635.
[19] Y. Zang, R.L. Street, J.R. Koseff, A dynamic mixed subgrid-scale model and its application to turbulent recirculating flows, Phys. Fluids A 5 (12) (1993) 3186–3196.
[20] U. Piomelli, J. Liu, Large eddy simulation of rotating channel flows using a localized dynamic model, Phys. Fluids 7 (4) (1995) 839–848.
[21] K. Horiuti, A new dynamic two-parameter mixed model for large-eddy simulation, Phys. Fluids 9 (11) (1997) 426–428.
[22] F.A. Jaberi, R.S. Miller, C.K. Madnia, P. Givi, Non-gaussian scalar statistics in homogeneous turbulence, J Fluid Mech. 313 (1996) 241–282.
[23] F.A. Jaberi, Temperature fluctuations in particle-laden homogeneous turbulent flows, Int. J. Heat Mass Transfer 41 (1998) 4081–4093.
[24] F.A. Jaberi, F. Mashayek, Temperature decay in two-phase turbulent flows, Int. J. Heat Mass Transfer 43 (2000) 993–1005.
[25] B. Vreman, B. Geurts, H. Kuerten, A priori tests of large eddy simulation of compressible plane mixing layer, J. Eng. Math. 29 (1995) 299–327.
[26] F.M. Najjar, D.K. Tafti, Study of discrete test filters and finite difference approximations for the dynamic subgrid-scale stress model, Phys. Fluids 8 (4) (1996) 1076–1088.
[27] Y. Zhou, M. Hossain, G. Vahala, A critical look at the use of filters in large eddy simulation, Phys. Lett. A 139 (7) (1989) 330–332.